

On a Thermodynamic Approach to Material Selection for Service in Aggressive Multi-Component Gaseous and/or Vapor Environments

Fuel Cycle Research & Development

Prepared for
U.S. Department of Energy
Used Fuel Disposition Campaign
M.V. Glazoff, S.C. Marschman, and
N. Soelberg
Idaho National Laboratory
September 21, 2015
FCRD-UFD-2015-000590



DISCLAIMER

This information was prepared as an account of work sponsored by an agency of the U.S. Government. Neither the U.S. Government nor any agency thereof, nor any of their employees, makes any warranty, expressed or implied, or assumes any legal liability or responsibility for the accuracy, completeness, or usefulness, of any information, apparatus, product, or process disclosed, or represents that its use would not infringe privately owned rights. References herein to any specific commercial product, process, or service by trade name, trade mark, manufacturer, or otherwise, does not necessarily constitute or imply its endorsement, recommendation, or favoring by the U.S. Government or any agency thereof. The views and opinions of authors expressed herein do not necessarily state or reflect those of the U.S. Government or any agency thereof.

On a Thermodynamic Approach to Material Selection for Service in Aggressive Multi-Component Gaseous and/or Vapor Environments

**M.V. Glazoff, Idaho National Laboratory
S.C. Marschman, Idaho National Laboratory
N. Soelberg, Idaho National Laboratory**

**Revision 0
September 21, 2015**

**Idaho National Laboratory
Idaho Falls, Idaho 83415**

<http://www.inl.gov>

**Prepared for the
U.S. Department of Energy
Office of Used Nuclear Fuel Disposition Research and Development
Under DOE Idaho Operations Office Contract DE-AC07-05ID14517**

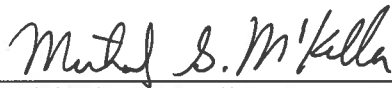
This page intentionally left blank.

On a Thermodynamic Approach to Material Selection for Service in Aggressive Multi-Component Gaseous and/or Vapor Environments

FCRD-UFD-2015-000590
INL/EXT-15-36724

Revision 0
September 21, 2015

Peer Review:



Michael G. McKellar
Idaho National Laboratory

September 21, 2015

Date

Submitted by:



Steven C. Marschman
Idaho National Laboratory

September 21, 2015

Date

This page intentionally left blank.

SUMMARY

This report fulfills the M4 milestone, M4FT-15IN08020110 UNF Analysis Support, under Work Package Number FT-15IN080201.

The issue of materials selection for many engineering applications represents an important problem, particularly in cases where material failure is possible as a result of corrosive environments. For example, 304 dual purpose or 316 stainless steel is used in the construction of many used nuclear fuel storage canisters. Deployed all over the world, these canisters are housed inside shielded enclosures and cooled passively by convective airflow. When located along seaboards or particular industrial areas, salt, other corrosive chemicals, and moisture can become entrained in the air that cools the canisters. It is important to develop an understanding of what impact, if any, that chemical environment will have on those canisters.

In many cases of corrosion in aggressive gaseous environments, the material selection process is based on some general recommendations, anecdotal evidence, and/or the past experience of that particular project's participants. For gaseous mixtures, the theoretical basis is practically limited to the construction of the so-called "Ellingham diagrams" for pure metals. These plots predict the equilibrium temperature between different individual metals, their respective oxides, and oxygen gas. Similar diagrams can be constructed for the reactions with sulfur, nitrogen, carbon, etc. In the generalization of this approach by Richardson and Jeffes, additional scales can be superimposed upon an Ellingham diagram that would correspond to different gaseous mixtures, e.g. CO/CO₂, or H₂/H₂O.

However, while the general approach to predicting the stability of a multi-component heterogeneous alloy (e.g., steel or a superalloy) in a multi-component aggressive gaseous environment was developed in very general form, actual examples of its applications to concrete real-life problems are practically absent. This is related to alloy design, corrosion protection, and material selection for different applications. In this work, an effort was made to advance in that direction using modern computational thermodynamics methodology, software, and databases by Thermo-Calc Inc. The developed methodology is illustrated by the case study – a process of nuclear waste immobilization using a chemical engineering approach described below. The developed methodology can be considered a practical illustration of the Ellingham approach generalization and could be used for obtaining thermodynamic guidance on a given process' feasibility using equipment/sensors made of a particular multicomponent heterogeneous metallic alloy.

CONTENTS

SUMMARY	vii
ACRONYMS	x
1. INTRODUCTION	1
2. DESCRIPTION OF THE PROPOSED APPROACH.....	3
3. A CASE STUDY: METAL ALLOY CORROSION IN A HIGH TEMPERATURE GASEOUS ENVIRONMENT	4
4. EXPERIMENTAL WORK: RAMAN SPECTROSCOPY, SCANNING ELECTRON MICROSCOPY, AND ENERGY DISPERSIVE SPECTROSCOPY	6
5. COMPUTATIONAL THERMODYNAMICS AND ASSESSMENT OF PROTECTIVE OXIDE LAYERS ON RA253MA AND SS316L STAINLESS STEELS.....	10
5.1 Thermodynamic Assessment Of Oxidation, Carburizing, and Sulfidation – Alloy RA253MA at 1000°C.....	10
5.2 Thermodynamic Assessment Of Oxidation, Carburizing, and Sulfidation – Stainless Steel 316 at 1000°C.....	12
5.3 Growth of Oxide Layers on Top of Stainless Steel 316 and Alloy Ra253MA; Their Protective / Passivating Properties	12
6. CONCLUSIONS AND PLANS FOR FUTURE RESEARCH.....	15
7. REFERENCES	16
Appendix 1 Thermo-Calc Script for Calculating Chemical Potentials of Several Components in Alloy RA253 MA	18
Appendix 2. Thermo-Calc Script for Calculating Chemical Potentials of Several Components in Gaseous Phase	18

FIGURES

Figure 1. The original Ellingham diagram [1].	2
Figure 2. The modified Ellingham - Richardson diagram illustrating oxidation of different chemical elements (Ni, Mo, Fe, Cr, Nb, Si, and Al) as a function of reciprocal temperature [9, 10]. Instead of the standard free energy of oxide formation, the partial pressure of oxygen is plotted at the “y”-axis.	2
Figure 3. View of the length of the probes.	4
Figure 4. Closer view of the two probes.	4
Figure 5. Raman spectroscopy analysis of a section of the unheated probe sheath.....	6

Figure 6. SEM micrograph at 46x magnification of the unheated probe sheath. 7

Figure 7. SEM micrograph at 42x magnification of the unheated probe sheath at another location. 8

Figure 8. SEM micrograph at 50x magnification of the heated probe sheath. 9

Figure 9. Formation of oxide layers on top of alloy SS316 at 800°C. The thermodynamic activity of oxygen (fugacity) is plotted along the x-coordinate, while BPW(*) stands for the weight fraction of the different phases comprising a given steel, and oxides forming on the surface. 13

Figure 10. Formation of oxide layers on top of alloy RA253MA at 800°C. The thermodynamic activity of oxygen (fugacity) is plotted along the x-coordinate, while BPW(*) stands for the weight fraction of the different phases comprising a given steel, and oxides forming on the surface. 14

Figure 11. Formation of oxide layers on top of stainless steel 316 at 1000°C. The thermodynamic activity of oxygen (fugacity) is plotted along the x-coordinate, while BPW(*) stands for the weight fraction of the different phases and oxides forming on the surface. 14

Figure 12. Formation of oxide layers on top of alloy RA253 MA at 1000°C. The thermodynamic activity of oxygen (fugacity) is plotted along the x-coordinate, while BPW(*) stands for the weight fraction of the different phases comprising a given steel, and oxides forming on the surface. 15

TABLES

Table 1. Elemental composition of unheated probe sheath, 46x magnification, metal body (“small tube spot”) from SEM/EDS analysis. 7

Table 2 Elemental composition of unheated probe sheath, 46x magnification, Spot 1 (inner corrosion layer) from SEM/EDS analysis. 7

Table 3 Elemental composition of unheated probe sheath, 46x magnification, Spot 2 (outer corrosion layer). 8

Table 4. Elemental composition of unheated probe sheath, 42x magnification, metal body (“small tube spot”). 8

Table 5. Elemental composition of unheated probe sheath, 42x magnification, larger corrosion layer (corrosion spot). 9

Table 6. Elemental composition of heated probe sheath, 50x magnification, metal body (“large tube spot”). 10

Table 7. Elemental composition of heated probe sheath, 50x magnification, corrosion spot 1. 10

Table 8. Elemental composition of heated probe sheath, 50x magnification, corrosion spot 2. 10

ACRONYMS

BWR	boiling water reactor
CANDU	Canada Deuterium Uranium
CRR	Carbon Reduction Reformer
EDS	energy dispersive x-ray spectroscopy
INL	Idaho National Laboratory
IWTU	Idaho Waste Treatment Unit
SEM	scanning electron microscopy

REGISTRATIONS AND TRADEMARKS

Hastelloy™ A registered trademark of Haynes International, Inc.

ON A THERMODYNAMIC APPROACH TO MATERIAL SELECTION FOR SERVICE IN AGGRESSIVE MULTI-COMPONENT GASEOUS AND/OR VAPOR ENVIRONMENTS

1. INTRODUCTION

The diagrams originally developed by Ellingham [1], give a possibility to compare the relative stability of different pure metals with respect to the processes of oxidation, formation of nitrides, carbides, sulfides, etc. Their later generalization by Richardson and Jeffes allows doing the same, but with mixtures of two different gases and their ratios as a variable (e.g., H₂/H₂O; CO/CO₂) [2]. This is achieved by adding a scale on the outside of the diagram so that the equilibrium partial pressures for H₂/H₂O vapor and/or CO/CO₂ could be read off the diagram similarly to the partial pressure of O₂. The result is a useful graphical compendium of thermodynamic data for many condensed metal/vapor reactions.

This group of methods turned out to be particularly useful in extractive metallurgy predicting how a given metal could be extracted from the ore most efficiently [3]. Such a success should be expected because an ore often represents an oxide of the extracted metal in mechanical mixture with smaller amounts of other oxides or different compounds. Then, a series of simple independent thermodynamic calculations allows selecting the most efficient reducing agent [4].

This is not so in the case of corrosion of multi-component, typically heterogeneous alloys such as steels or superalloys in aggressive gaseous environment comprised of a number of different gases interacting with the alloy material and in the gaseous phase. A metallic alloy is not a mechanical mixture of independent components but a non-ideal system that requires much more complex thermodynamic models for its adequate description. Currently used models include polynomial expansions with respect to temperature and concentration of components (often orthogonal polynomials are used for numerical stability purposes), sublattice models, associated solutions [5-7] and so on. At elevated temperatures, gases interact with each other according to the thermodynamic and kinetic rules, changing their relative composition because of these interactions and also because of possible reactions with the alloy material.

Perhaps Gaskell [8] was the first to realize this fact and discuss it as the problem of “non-standard states”. In his elegant approach it was proposed to account for non-ideality of a particular metal in a given metallic alloy in the following form. Because metal M is now in a non-ideal alloy (e.g., in solid solution), its ability to react and form a chemical compound with the gaseous environment *is reduced* and should be characterized by its activity. This affects the free energy change for the reaction (which is no longer the *standard* free energy change) and means that the pressure of reacting gas required for equilibrium between the metal in solution and the pure product is changed. These values can be found by substituting the modified activity of the metal into the expression for the equilibrium constant and ΔG . Indeed, in the case of a pure metal M we had the following relationship:

$$\Delta G_0 = -RT \ln K_{eq} \quad (1)$$

where ΔG_0 is the standard free of formation and K_{eq} stands for the equilibrium constant representing the partial pressures of the reacting gases. Now, for a non-ideal alloy expression (1) no longer holds, and the need arises to account for deviations from ideal behavior of the component M. This is achieved by using the following modified expression [8]:

$$\Delta G = \Delta G_0 - RT \ln a_M \quad (2)$$

where a_M is the thermodynamic activity of the component M in our multi-component alloy. As it was pointed out in [8], the decrease in activity may be interpreted graphically as rotating the Ellingham line for the reaction counter-clockwise around its intersection with $T = 0$.

For pure components, one can construct the Ellingham-Richardson diagrams, or modified diagrams, as shown below. In particular, in Figure 1 the original diagram of Ellingham the dissociation stability of different oxides is examined as a function of the oxygen partial pressure and reciprocal temperature [1].

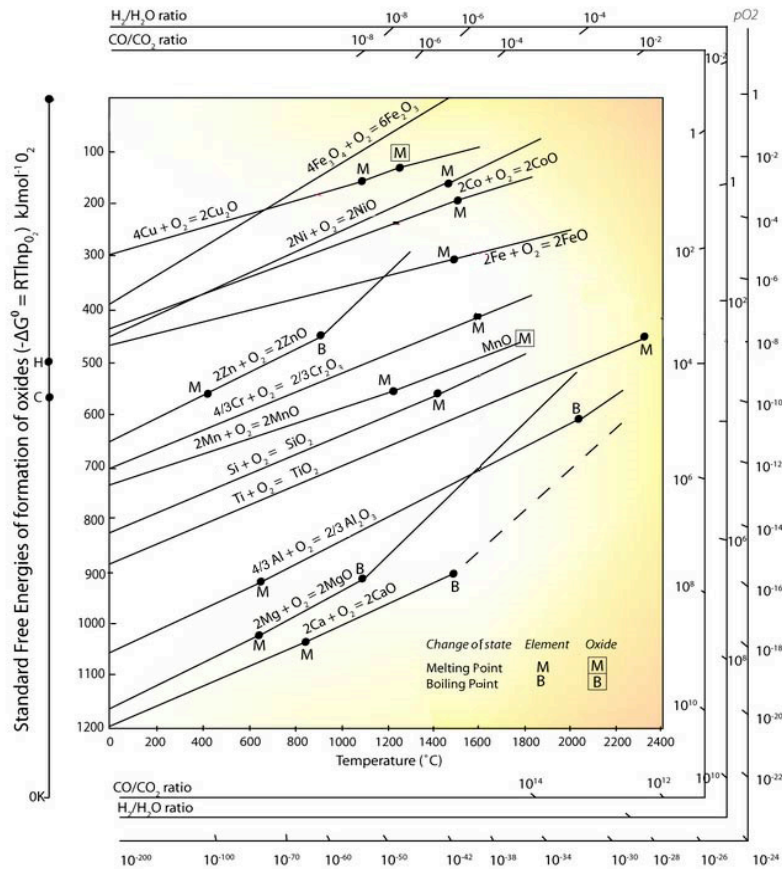


Figure 1. The original Ellingham diagram [1].

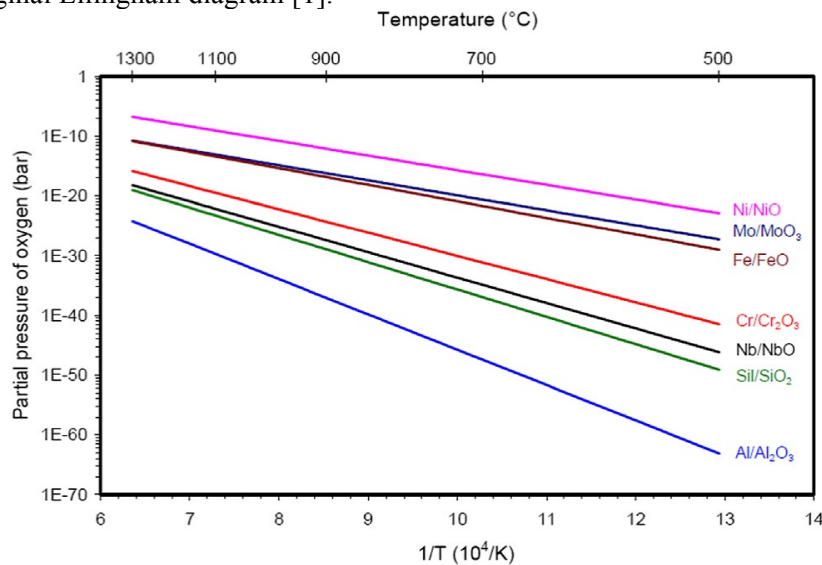


Figure 2. The modified Ellingham - Richardson diagram illustrating oxidation of different chemical elements (Ni, Mo, Fe, Cr, Nb, Si, and Al) as a function of reciprocal temperature [9, 10]. Instead of the standard free energy of oxide formation, the partial pressure of oxygen is plotted at the “y”-axis.

For multi-component materials these calculations become much more difficult. Equation (2), in spite of its seeming simplicity, is never used in practice of corrosion assessment for alloys in aggressive gaseous mixtures, or for material selection for a particular application, or for alloy design. This is because one needs to give clear answers to a number of important questions:

1. For a given multicomponent homogeneous alloy (e.g., solid solution), it is necessary to calculate the activities of all alloying elements as functions of temperature and composition of the gaseous phase;
2. For a heterogeneous multi-component alloy, it becomes necessary to assess the corresponding dependencies for each component in each of the phases comprising a given alloy at given conditions;
3. The equilibrium composition of the gaseous phase needs to be computed for the temperature range of interest (and, possibly, varying external pressure);
4. Based upon these calculations one needs to assess whether conditions exist for such detrimental processes as oxidation, formation of nitrides, carbides, sulfides, etc.
5. If oxidation is thermodynamically possible, it becomes necessary to calculate the composition of the oxide layers on top of the alloy surface and assess their passivation or protection potential against further unchecked corrosion.

2. DESCRIPTION OF THE PROPOSED APPROACH

At first, the problem seems to be pretty straightforward. Compute thermodynamic equilibrium in metallic alloy; then use chemical thermodynamics to compute equilibrium in the gaseous phase, and after that – bring the two systems together and try to find the global equilibrium of this combined system. Analyze its composition and, if oxides, sulfides, carbides etc. are present, make a conclusion about the thermodynamically possible corrosion reactions of the selected material at a given set of conditions.

In reality, there are complications making this set of instructions impossible to execute. One issue is that the same chemical element can enter both a compound in the gaseous phase and the solid (liquid) alloy. Then, it becomes practically impossible to define a standard state for said component. Secondly, a particular chemical element comprising the solid alloy may react with e.g. oxygen forming solid oxide scale on the alloy surface. In this case the standard state of oxygen is also impossible to define without any ambiguity, and any thermodynamic calculations become impossible.

As a result, the following approach was developed based on the application of chemical potentials of components, rather than their concentrations, see below.

1. Calculate the chemical potentials of all components of interest in the selected solid alloy at a given temperature and external pressure. Typically, if one considers selecting steel or a superalloy for a particular application, these components will be iron Fe, nickel Ni, chromium Cr, possibly molybdenum Mo, silicon Si, sulfur S, and carbon C;
2. Compute the chemical potentials of the elements comprising a gaseous phase. These, depending upon the problem at hand, might be carbon C, hydrogen H₂, nitrogen N₂, sulfur S, oxygen O₂, etc. Depending upon the difference of chemical potentials in the gaseous and in the solid phase, make conclusions about a possibility of these elements reacting with metallic alloy of choice;
3. Using thermodynamic tables or databases [11], calculate the free energy of formation of the several oxides (sulfides, carbides, etc.) that could potentially represent a problem in oxidation/corrosion of the selected metallic alloys. This needs to be done at the actual temperature and pressure of the process;
4. Use the actual values of the element chemical potential(s) in considered alloy to introduce correction to the value of ΔG_0 using expression below (in which chemical potentials μ_A and

μ_B are calculated for components A and B in the considered metallic alloy, while the values of $\Delta G_{A_m B_n}$ and $\Delta G_{0, A_m B_n}$ are calculated for the temperature of experiment, T):

$$\Delta G_{A_m B_n} = \Delta G_{0, A_m B_n} - m\mu_A - n\mu_B \quad (3)$$

5. Depending upon the sign and value of the obtained results for ΔG , make conclusions about the possibility of oxidation (sulfidation, carburizing etc.) for the selected alloy.

We note that this program becomes possible only when using modern thermodynamic computational engines such as Thermo-Calc, plus extensive thermodynamic databases.

In the next section two alloys are considered that were used for manufacturing oxygen probes in a nuclear waste stabilization process. Both alloys failed, and it was necessary to answer the following questions. First, what was the nature of that corrosion attack? Secondly, what could be done in the future to prevent such corrosion attacks? Finally, which material would be appropriate in the harsh conditions of the immobilization process?

3. A CASE STUDY: METAL ALLOY CORROSION IN A HIGH TEMPERATURE GASEOUS ENVIRONMENT

Two metallic in situ O₂ probes were analyzed during late August and early September 2014 to evaluate the cause(s) of corrosion on these probes and make recommendations for how this corrosion could be mitigated. These probes penetrated through the refractory-lined piping at the outlet of Carbon Reduction Reformer (CRR), which is a component of the Idaho Waste Treatment Unit (IWTU). The IWTU is undergoing startup operations preparatory to operating this facility to convert liquid radioactive sodium bearing waste at the Idaho National Laboratory (INL) into a granular solid material using steam reforming. The CRR oxidizes the process gas to destroy incompletely oxidized organic compounds, H₂, and CO in order to comply with air emissions requirements. The two O₂ probes were exposed oxidizing conditions at temperatures up to 950°C, and reducing conditions at temperatures up to about 350°C. These probes had failed to respond (provide valid O₂ measurements) and were removed from their sampling locations in the off-gas piping. When they were removed, corrosion on the probes was evident (see Figures 1 and 2).



Figure 3. View of the length of the probes.



Figure 4. Closer view of the two probes.

The larger-diameter probe is the heated probe. The smaller-diameter probe is unheated. The sheath on the heated probe has been completely corroded away on the leading edge (the side facing into the process gas flow). Exposed metal portions of the assembly of the heated probe have also been significantly corroded, especially the cotter pin and washer on the end of the probe heater. The sheath on the heating coil of the heated probe appears intact and corrosion resistant, even though this metal was exposed to the most severe conditions, exposed to the hot gas and also internally heated to about 700°C.

The most severe corrosion was on the sheath of the heated probe made of stainless steel 316. Less corrosion was found on the unheated probe sheath, which was made of RA 253 MA alloy. Until this corrosion incident, it was widely considered that this alloy had good resistance to oxidation at temperatures up to 1,100°C, and to sulfidation under oxidizing conditions at temperatures up to 1,000°C, but only fair resistance to carburization (which requires higher nickel content), and it is not resistant to sulfidation under reducing conditions.

Conditions these probes were exposed to included four general operating regimes.

- Regime 1: Temperatures from ambient to about 100-200°C. Potential range of approximate gas composition: 0-1% O₂, 0-5% CO₂, 0-1% H₂O, 0-50 ppm total S species ranging between H₂S to SO₂, 0-1 ppm SO₃. Balance N₂.
- Regime 2: 200-350°C. Potential range of approximate gas composition: Same as Regime 1.
- Regime 3: 350-950°C. Potential range of approximate gas composition: 3-5% O₂, 10% CO₂, 1-5% H₂O, 50-100 ppm SO₂, 1-2 ppm SO₃, <100 ppm CO and <1,000 ppm NO_x. Balance N₂.
- Regime 4: 950°C. Potential range of approximate gas composition: 3-5% O₂, 10% CO₂, ~50% H₂O, 50-100 ppm SO₂, 1-2 ppm SO₃, <100 ppm CO, and <1,000 ppm NO_x. Balance N₂.

Particulate matter entrained in the gas stream was not high, although there were some entrained bauxite particles, particles of petroleum coke, and particles of coke fly ash. All particles were likely under 10-100 micron. This includes:

- About 100-500 mg/m³ bauxite particles (mainly alumino-silicate), calculated from approximate bauxite elutriation rates.
- About 1,000 - 5,000 mg/m³ fine, unoxidized petroleum coke particles, calculated based on the range of excess amount fed to the CRR and not oxidized.
- About 30 mg/m³ fly ash particles from petroleum coke oxidation.
- The total amount of particulate matter, rounded to one significant figure: 1,000 to 5,000 mg/m³ (0.5 to 2.5 grain/ft³) particulate matter.

The entrained particulate matter is not expected to generally reach softening/slagging temperatures for these materials. The off-gas velocity at this location ranged from 30 to 100 fps. Therefore, it is possible that the entrained particulate matter may have been slightly erosive to the exposed probe sheath. This may be a particular issue for the heated probe where even minor levels of erosion may have interfered with stable oxide film growth on the surface of the metal, which would have further accelerated the oxidation corrosion mechanism on the heated probe.

Visual inspection, scanning electron microscopy (SEM) and energy dispersive x-ray spectroscopy (EDS), Raman spectroscopy, and computational thermodynamics and corrosion modeling were performed. These analyses and modeling indicated that the corrosion to the probe sheaths was caused by oxidation, and not any other forms of attack such as sulfidation or carburization. It was also proposed that other alloys that might perform as well or better than RA253MA include RA333 (works in ambient atmosphere up to 1200°C) Alloy X, Alloy 600, or alloy RA602CA [12]. These results are discussed in the next section.

4. EXPERIMENTAL WORK: RAMAN SPECTROSCOPY, SCANNING ELECTRON MICROSCOPY, AND ENERGY DISPERSIVE SPECTROSCOPY

Raman Spectroscopy. After the preceding photos were taken, the probes were analyzed using Raman spectroscopy and SEM/EDS analysis. Raman spectroscopy was performed in an attempt to determine if carbon was present in the corrosion layers. The results indicated that little or no free carbon was present, because there were no peaks at wavenumbers indicative of carbon in Figure 5. This indicates that carburization attack could not have been the cause or a significant contributor to the corrosion.

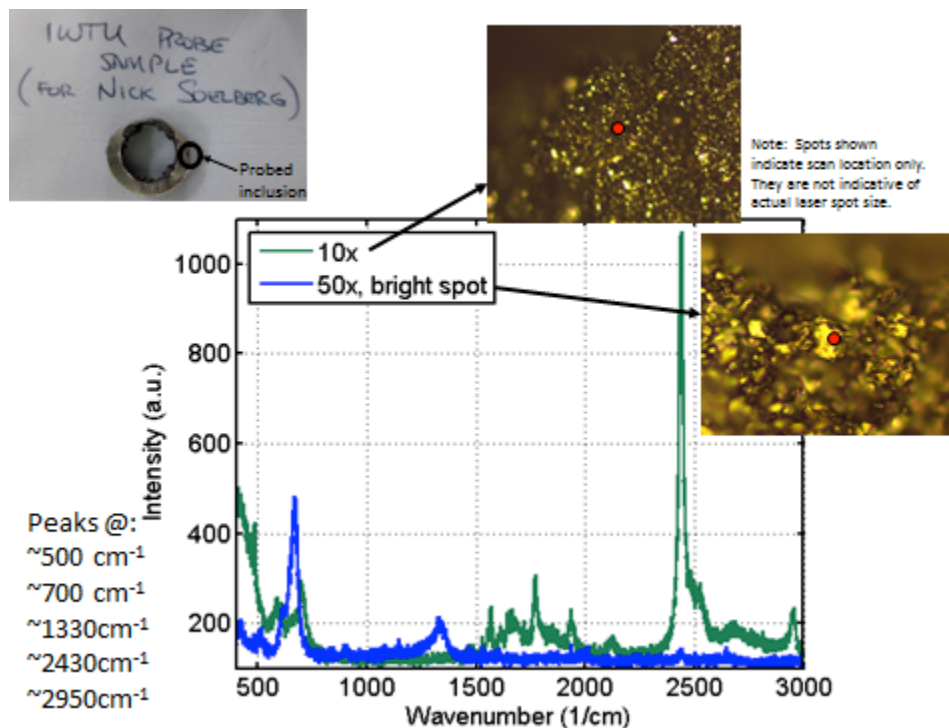


Figure 5. Raman spectroscopy analysis of a section of the unheated probe sheath.

Figure 6 shows an SEM photomicrograph of the sheath of the unheated tube, with corrosion spots on both outer and inner surfaces. Results of EDS analyses (Tables 1, 2, and 3) show the elemental compositions of the three spots shown in this figure. The metal of this sheath is an Fe-Cr-Ni-Si-Mn alloy, consistent with the RA233MA composition, which has, along with Fe, about 20 wt% Cr, 10 wt% Ni, 1-2 wt% Si, >0.8 wt% Mn, and smaller amounts of N, Ce, P, and S. In this and other EDS composition tables, the amount of C indicated is biased upward due to the carbon coating on the samples. The two corrosion layer compositions have elevated oxygen, indicating oxygen attack, but not elevated S, N, or C, Na, Ca, K, or Si, that could, if present, indicate other forms of corrosive attack.

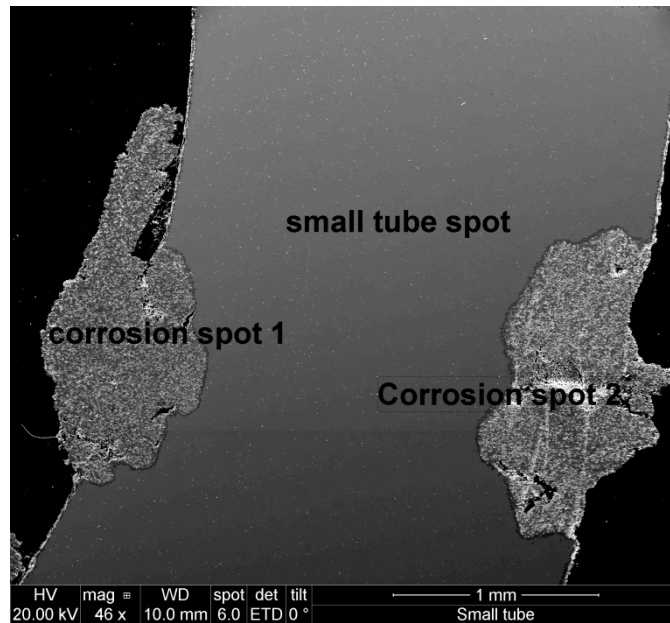


Figure 6. SEM micrograph at 46x magnification of the unheated probe sheath.

Table 1. Elemental composition of unheated probe sheath, 46x magnification, metal body (“small tube spot”) from SEM/EDS analysis.

Element	Wt %	At %	K-Ratio	Z	A	F
C K	3.98	15.15	0.0083	1.1693	0.1791	1.0004
O K	1.90	5.44	0.0084	1.1492	0.3827	1.0034
SiK	1.82	2.97	0.0091	1.0990	0.4509	1.0013
CrK	19.09	16.81	0.2130	0.9815	0.9915	1.1463
MnK	0.80	0.66	0.0077	0.9645	0.9976	1.0100
FeK	62.58	51.30	0.6038	0.9834	0.9687	1.0128
NiK	9.82	7.66	0.0890	1.0002	0.9056	1.0000
Total	100.00	100.00				

Table 2 Elemental composition of unheated probe sheath, 46x magnification, Spot 1 (inner corrosion layer) from SEM/EDS analysis.

Element	Wt %	At %	K-Ratio	Z	A	F
C K	4.49	13.69	0.0106	1.1486	0.2053	1.0005
O K	13.95	31.97	0.0632	1.1289	0.4001	1.0026
CeM	1.12	0.29	0.0021	0.8366	0.2289	1.0000
AlK	0.15	0.21	0.0006	1.0498	0.3579	1.0007
SiK	0.15	0.19	0.0008	1.0800	0.4810	1.0014
CaK	0.20	0.18	0.0021	1.0558	0.9400	1.0444
V K	1.09	0.78	0.0111	0.9451	0.9896	1.0889
CrK	19.67	13.87	0.2136	0.9628	0.9971	1.1309
MnK	0.60	0.40	0.0057	0.9459	0.9981	1.0013
FeK	57.38	37.66	0.5361	0.9642	0.9673	1.0016
NiK	1.20	0.75	0.0107	0.9803	0.9108	1.0000
Total	100.00	100.00				

Table 3 Elemental composition of unheated probe sheath, 46x magnification, Spot 2 (outer corrosion layer).

Element	Wt %	At %	K-Ratio	Z	A	F
C K	3.39	10.01	0.0080	1.1431	0.2060	1.0005
O K	17.35	38.50	0.0841	1.1235	0.4304	1.0025
AlK	0.14	0.19	0.0005	1.0449	0.3617	1.0007
SiK	0.16	0.20	0.0008	1.0750	0.4859	1.0013
V K	0.65	0.45	0.0066	0.9402	0.9915	1.0945
CrK	18.96	12.95	0.2067	0.9578	0.9985	1.1396
MnK	0.58	0.38	0.0055	0.9408	1.0018	1.0011
FeK	57.79	36.74	0.5395	0.9590	0.9721	1.0014
NiK	0.98	0.59	0.0087	0.9748	0.9133	1.0000
Total	100.00	100.00				

Figure 11 shows another location on the unheated probe sheath, with a larger mass of corrosion layer or deposit. The elemental composition of the metal in this figure (Table 4) is essentially identical to that in the prior figure. The elemental composition of the corrosion layer in this figure (Table 5) is also essentially identical to the corrosion layers in the prior figure.

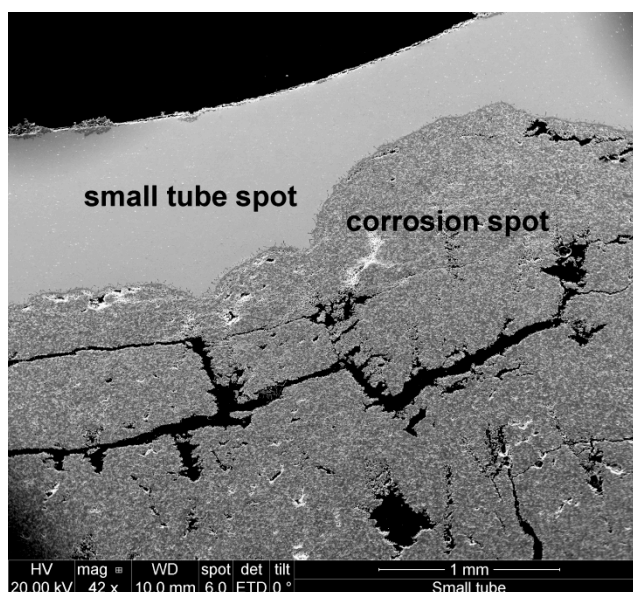


Figure 7. SEM micrograph at 42x magnification of the unheated probe sheath at another location.

Table 4. Elemental composition of unheated probe sheath, 42x magnification, metal body (“small tube spot”).

Element	Wt %	At %	K-Ratio	Z	A	F
C K	3.31	12.89	0.0069	1.1712	0.1781	1.0004
O K	1.86	5.43	0.0083	1.1510	0.3870	1.0034
SiK	1.65	2.76	0.0082	1.1007	0.4475	1.0013
CrK	18.30	16.49	0.2053	0.9833	0.9911	1.1510
MnK	0.79	0.67	0.0077	0.9662	0.9973	1.0101
FeK	64.09	53.76	0.6203	0.9851	0.9698	1.0130
NiK	10.01	7.99	0.0907	1.0020	0.9044	1.0000
Total	100.00	100.00				

Table 5. Elemental composition of unheated probe sheath, 42x magnification, larger corrosion layer (corrosion spot).

Element	Wt %	At %	K-Ratio	Z	A	F
C K	2.90	8.98	0.0068	1.1485	0.2028	1.0005
O K	15.04	34.98	0.0666	1.1289	0.3912	1.0025
SiK	0.31	0.41	0.0016	1.0800	0.4817	1.0014
CaK	0.42	0.39	0.0043	1.0558	0.9404	1.0444
V K	2.24	1.64	0.0229	0.9450	0.9893	1.0918
CrK	18.65	13.35	0.2032	0.9627	0.9968	1.1356
MnK	0.56	0.38	0.0053	0.9457	0.9973	1.0018
FeK	58.18	38.78	0.5448	0.9640	0.9692	1.0023
NiK	1.71	1.08	0.0152	0.9800	0.9112	1.0000
Total	100.00	100.00				

Figure 8 shows an SEM photomicrograph of the sheath of the heated tube, with corrosion spots on both outer and inner surfaces. Results of EDS analyses shown in Tables 6, 7, and 8 show the elemental compositions of the three spots shown in this figure. The metal of this sheath is an Fe-Cr-Ni-Mo-Mn-Si alloy, consistent with 316 stainless steel composition, which along with Fe contains about 17 wt% Cr, 12 wt% Ni, 2.5 wt% Mo, 2 wt% Mn, and 1 wt% Si. The two corrosion layer compositions have elevated oxygen, but not elevated S, N, or C, Na, Ca, K, or Si, that could, if present, indicate other forms of corrosive attack.

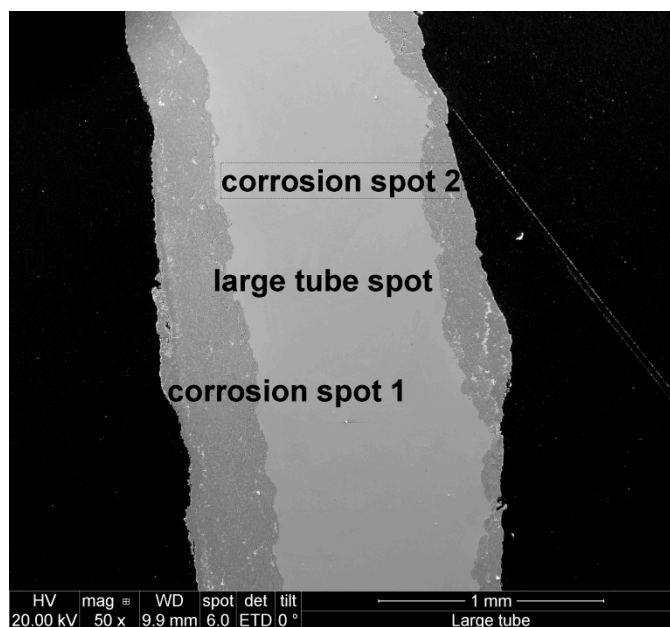


Figure 8. SEM micrograph at 50x magnification of the heated probe sheath.

This sheath appears to have formed a very brittle FeCrMo (Ni) phase called SIGMA, at the high operating temperatures up to 1,000°C, which are too high for this 316 SS sheath. The maximum operating temperature for steel 316 SS is about 800°C or even lower. As a matter of fact, it could be 650°C, due to the scale formation.

The start-up sequence includes periods of reducing (no free O₂ with presence of H₂S) and oxidizing (free O₂ of ~1 to 5 vol% O₂ and some SO_x). The alternating reducing/oxidizing conditions may impact the formation of a protective oxide layer, which might have affected corrosion on both probes.

Table 6. Elemental composition of heated probe sheath, 50x magnification, metal body (“large tube spot”).

Element	Wt %	At %	K-Ratio	Z	A	F
C K	2.99	12.44	0.0062	1.1791	0.1749	1.0004
SiK	0.88	1.57	0.0043	1.1079	0.4434	1.0017
MoL	1.97	1.03	0.0142	0.8936	0.8035	1.0017
CrK	16.87	16.21	0.1904	0.9904	0.9875	1.1543
MnK	1.12	1.02	0.0109	0.9733	0.9945	1.0089
FeK	67.00	59.94	0.6526	0.9924	0.9701	1.0117
NiK	9.16	7.80	0.0833	1.0097	0.9007	1.0000
Total	100.00	100.00				

Table 7. Elemental composition of heated probe sheath, 50x magnification, corrosion spot 1.

Element	Wt %	At %	K-Ratio	Z	A	F
C K	3.59	10.97	0.0070	1.1403	0.1711	1.0004
N K	3.37	8.85	0.0090	1.1301	0.2349	1.0011
O K	10.62	24.40	0.0381	1.1207	0.3191	1.0020
SiK	3.17	4.15	0.0161	1.0722	0.4714	1.0017
P K	0.91	1.08	0.0055	1.0439	0.5745	1.0026
MoL	3.05	1.17	0.0214	0.8612	0.8131	1.0015
CrK	14.94	10.56	0.1549	0.9562	0.9871	1.0982
MnK	0.47	0.31	0.0045	0.9394	0.9942	1.0376
FeK	32.14	21.15	0.3141	0.9577	0.9734	1.0484
NiK	27.73	17.36	0.2555	0.9738	0.9462	1.0000
Total	100.00	100.00				

Table 8. Elemental composition of heated probe sheath, 50x magnification, corrosion spot 2.

Element	Wt %	At %	K-Ratio	Z	A	F
C K	2.62	7.70	0.0056	1.1387	0.1867	1.0005
N K	4.44	11.19	0.0130	1.1285	0.2594	1.0012
O K	14.03	30.94	0.0524	1.1192	0.3327	1.0020
SiK	1.36	1.71	0.0070	1.0708	0.4814	1.0017
P K	0.15	0.17	0.0009	1.0420	0.5951	1.0031
MoL	3.33	1.22	0.0241	0.8594	0.8419	1.0019
CrK	18.72	12.70	0.1937	0.9545	0.9905	1.0948
MnK	0.60	0.39	0.0058	0.9377	0.9968	1.0256
FeK	35.05	22.14	0.3351	0.9559	0.9690	1.0321
NiK	19.69	11.83	0.1798	0.9719	0.9396	1.0000
Total	100.00	100.00				

Thus, these analyses show that the only type of corrosion attack in all cases on both probes was uncontrolled oxidation. Below, we use the methods of computational thermodynamics to substantiate this statement.

5. COMPUTATIONAL THERMODYNAMICS AND ASSESSMENT OF PROTECTIVE OXIDE LAYERS ON RA253MA AND SS316L STAINLESS STEELS

5.1 Thermodynamic Assessment Of Oxidation, Carburizing, and Sulfidation – Alloy RA253MA at 1000°C

This work was done for steel 316 SS and steel RA253MA using the step-by-step program of calculations outlined in Section 1. In order to compute the required chemical potential of different components in solid and gaseous phases, and the values of $\Delta G_{0,A_m B_n}$ and $\Delta G_{A_m B_n}$, it is necessary to use both a reliable

thermodynamic computational engine allowing solving for global equilibrium for multi-component heterogeneous systems, and the corresponding thermodynamic databases. In our case, Thermo-Calc v.3.1 software was used with thermo-dynamic databases TCFE7 (for Fe-based alloys) and SSUB5 (for different chemical substances), all produced by Thermo-Calc Software AB company. Scripts were written in Thermo-Calc programming meta-language and run using these databases. Note that Ce, a component of the RA253MA steel, was not considered since it is not yet included in TCFE7. Yet, very convincing results were obtained.

By running the steel.tcm Thermo-Calc script (Appendix 1), the following chemical potentials of Fe, Cr, Ni, Si and C in steel were calculated, in J/mole:

$$\begin{aligned} \mu(Fe) &= -4266; & \mu(Cr) &= -9836; & \mu(Ni) &= -29316 \\ \mu(Si) &= -143705; & \mu(C) &= -51880 \end{aligned} \quad (4)$$

On the other hand, by running the script gas.tcm (Appendix 2), the chemical potentials of C, O and S in the gaseous phase were calculated, in J/mole:

$$\mu(C) = -406,675; \quad \mu(O) = -17,042; \quad \mu(S) = -332,401 \quad (5)$$

From these calculations, it can be seen that the chemical potential of C in the gaseous phase is much lower than that in steel. Therefore, no carburization should occur, which is in agreement with our experimental observations.

Using the TAB module of ThermoCalc and SSUB5 database [11], the standard Gibbs free energy change of four oxidation reactions at T=1273 K can be calculated:

1. $O_2 + Si = SiO_2$ $dG_0 = -6.83047 \cdot 10^5$
2. $Ni + 0.5O_2 = NiO$ $dG_0 = -1.26745 \cdot 10^5$
3. $Fe + 0.5O_2 = FeO$ $dG_0 = -1.90713 \cdot 10^5$
4. $Cr + 0.75O_2 = 0.5Cr_2O_3$ $dG_0 = -4.03644 \cdot 10^5$

Taking into account the actual chemical potentials of Si, Ni, Fe, Cr and O, the Gibbs free energy changes were updated accordingly:

1. $O_2 + Si = SiO_2$ $dG = dG_0 - 2 \cdot \mu(O) - \mu(Si) = -505258$
2. $Ni + 0.5O_2 = NiO$ $dG = dG_0 - \mu(O) - \mu(Ni) = -80387$
3. $Fe + 0.5O_2 = FeO$ $dG = dG_0 - \mu(O) - \mu(Fe) = -169404$
4. $Cr + 0.75O_2 = 0.5Cr_2O_3$ $dG = dG_0 - 1.5 \cdot \mu(O) - \mu(Cr) = -368244$

Thus, thermodynamic calculations indicate that Si, Ni, Fe and Cr in the steel can all be oxidized by the flowing gas mixture. In reality, however, which oxides will be formed also depends on the kinetics of the competing processes.

Performing similar calculations for the sulfidation reactions, we got the following results:

1. $Cr + 0.5S_2 = CrS$ $dG_0 = -1.14983 \cdot 10^5$ $dG = dG_0 - \mu(Cr) - \mu(S) = +227,466$
2. $Fe + 0.5S_2 = FeS$ $dG_0 = -8.28077 \cdot 10^4$ $dG = dG_0 - \mu(Fe) - \mu(S) = +25,4071$
3. $3Ni + S_2 = Ni_3S_2$ $dG_0 = -1.57353 \cdot 10^5$ $dG = dG_0 - 3 \cdot \mu(Ni) - 2 \cdot \mu(S) = +59,5819$

All these reactions have positive free energy change. Therefore, sulfidation should not occur under these experimental conditions, which agrees with our experimental data.

5.2 Thermodynamic Assessment Of Oxidation, Carburizing, and Sulfidation – Stainless Steel 316 at 1000°C

We performed the same algorithm using the scripts for steel (steel.tcm) and gaseous phase (gas.tcm), and introducing the necessary changes into the values of concentrations of different components in SS316 compared to RA253MA. As expected, we got similar results: no possibility of sulfidation or carburizing, only oxidation was thermo-dynamically possible at 1000°C.

5.3 Growth of Oxide Layers on Top of Stainless Steel 316 and Alloy Ra253MA; Their Protective / Passivating Properties

The formation of different protective layers (in many cases – Cr_2O_3 or double oxides of the spinel type) is what makes stainless steel truly stainless. The stability of surface oxides provides the passivity of aluminum or zirconium to oxidation at room temperature, which is otherwise possible thermodynamically [13]. Among the factors that facilitate corrosion (especially of the pitting type) is the formation of sharp second phase particles (precipitates, dispersoids, or constituent particles) [14]. These particles, depending upon their chemical composition, could be anodic or cathodic with respect to the solid solution matrix [15]. In both cases, this could result either in the dissolution of the particle itself (e.g., Mg_2Si dispersoids in AA6061-T6 aluminum saturated solid solution matrix, or in the latter case – the matrix itself would get eroded. The material can become even more corrosion-prone in the case of sharp particles piercing the oxide protective layers, be it engineered structures like a thin layer of boehmite in nuclear aluminum alloys, or naturally growing oxide layers, e.g., in stainless steels. It was known for quite a long time that sharp particles of MnS forming in stainless steel serve as potential center for pitting corrosion. The same is true for carbides M_{23}C_6 and M_3C (with $\text{M}=\text{Fe}, \text{Cr}, \text{Ni}$), nitrides etc. [16]

Furthermore, one can speculate that the release of gaseous materials from alloys should be considered unacceptable when analyzing the stability of surface passivating layers.

In some cases, especially in steels and/or superalloys, a protective oxide layer actually can be comprised of the two layers, one on the top of the other, [17]. For example, in SS and nickel alloys a passivating layer of spinel chromite (typically FeCr_2O_4) is formed directly on the alloy surface. On top of this passivating layer another layer of coarser crystallites (ca. 1 μm) of the inverse spinel ferrite (non-stoichiometric $\text{Ni}_x\text{Fe}_{3-x}\text{O}_4$, with $x\sim 0.6$) [18] can deposit. In the case of boiling water reactors (BWRs) chromite is practically not formed as it is washed off by the oxidizing coolant which contains soluble Cr^{6+} [18]. On the other hand, in these materials the formation of ferritic oxides (haematite $\alpha\text{-Fe}_2\text{O}_3$ and maghemaetite $\gamma\text{-Fe}_2\text{O}_3$) on top of the outer layer is possible. In CANada Deuterium Uranium (CANDU) reactors, where some reactor components are made of carbon steel, the formation of the double protective layer of magnetite, Fe_3O_4 , is the principal mechanism of protection against unchecked corrosion. In the most general case of corrosion in electrolyte environments (most typically, aqueous) the construction of Pourbaix diagrams for real steels/nickel alloys in real environments (including the composition of the gaseous / vapor phase) seems to be highly desirable. As a general rule, however, it is always necessary to take into consideration the composition of the environment and the considered alloy quantitatively. This is now possible with the development of computational thermodynamics and thermodynamics of electrolytes (including ionic liquids, see examples at [19, 20]).

With these general considerations in mind, we can analyze the oxide layer diagrams on the two materials of interest in this particular work - stainless steel SS316 and alloy RA253MA. Two temperatures were selected corresponding to the case of the most aggressive environments – 800°C and 1000°C. We used the modified Thermo-Calc scripts for these analyses [11]. In order to probe the relative stability of oxides forming on these two types of steel, we performed computational thermodynamics calculations using software Thermo-Calc v.3.1 and the TTFE7 database. The results are presented in Figures 7 and 8 (800°C); and 9 and 10 (1000°C), respectively.

Figure 7 for 800°C shows that at the lowest possible activity of oxygen in our computational experiment ($\ln\{a_{O_2}\} = -28$) the formation of MnS precipitates takes place in SS316, followed by the appearance of the surface layer of tephroite, Mn_2SiO_4 . As discussed above, the initial appearance of sharp precipitates, rather than double oxide layers, is detrimental for corrosion resistance of any material. Also, it is doubtful that such an oxide as Mn_2SiO_4 (appearing at $\sim \ln\{a_{O_2}\} = 10^{-27}$) is capable of passivating the surface; no data of that nature could be found in the literature. The appearance of these two substances already clearly indicates that SS316 will fail on the particular aggressive atmosphere described above, even at 800°C.

In the case of alloy RA253MA, the formation of the protective surface layer of Cr_2O_3 takes place at $\ln\{a_{O_2}\} = -22$, while for SS 316L, only at $\ln\{a_{O_2}\} = -21$, or one order of magnitude higher. However, at similar oxygen activities the formation and subsequent dissolution (at higher oxygen concentrations) of M23C6 carbide is probably not very good for protection against corrosion, and the first oxide to form on the surface is β - SiO_2 , not Cr_2O_3 or any spinel. This means that the RA253MA steel will work somewhat better and sustain less corrosion and scaling than 316L, but both materials are not suitable for exposure above 800°C for the particular type of aggressive gaseous atmosphere considered in this paper.

At 1000°C passivation is worse than at 800°C. For SS316 the formation of MnS still takes place first, disqualifying this material for service, while for RA253MA tridymite (a high temperature polymorph of silica) is formed, the protection properties of which are not well studied. Consequently, neither material are impervious to corrosion at the harsh conditions (high temperature, aggressive gaseous atmosphere) in this case study.

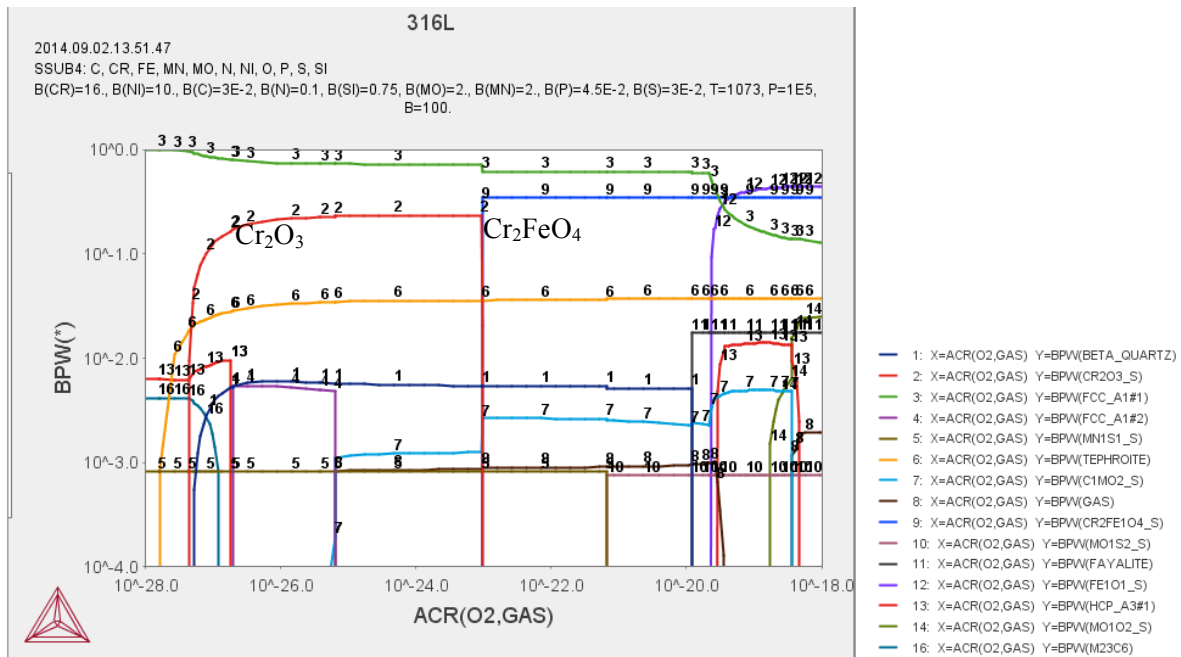


Figure 9. Formation of oxide layers on top of alloy SS316 at 800°C. The thermodynamic activity of oxygen (fugacity) is plotted along the x-coordinate, while BPW(*) stands for the weight fraction of the different phases comprising a given steel, and oxides forming on the surface.

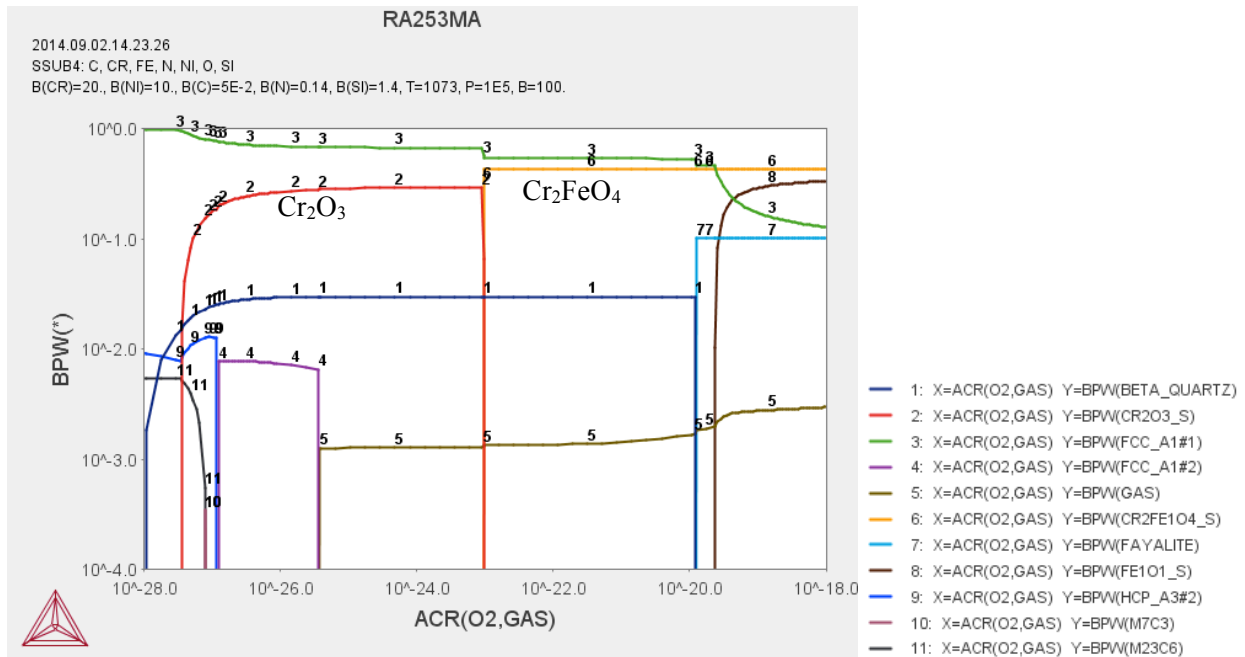


Figure 10. Formation of oxide layers on top of alloy RA253MA at 800°C. The thermodynamic activity of oxygen (fugacity) is plotted along the x-coordinate, while BPW(*) stands for the weight fraction of the different phases comprising a given steel, and oxides forming on the surface.

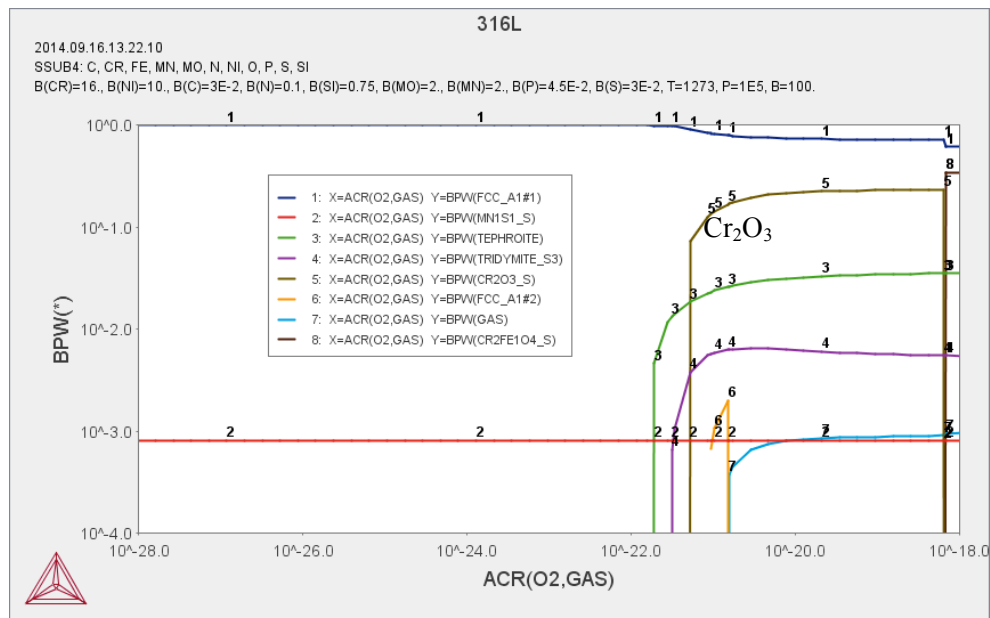


Figure 11. Formation of oxide layers on top of stainless steel 316 at 1000°C. The thermodynamic activity of oxygen (fugacity) is plotted along the x-coordinate, while BPW(*) stands for the weight fraction of the different phases and oxides forming on the surface.

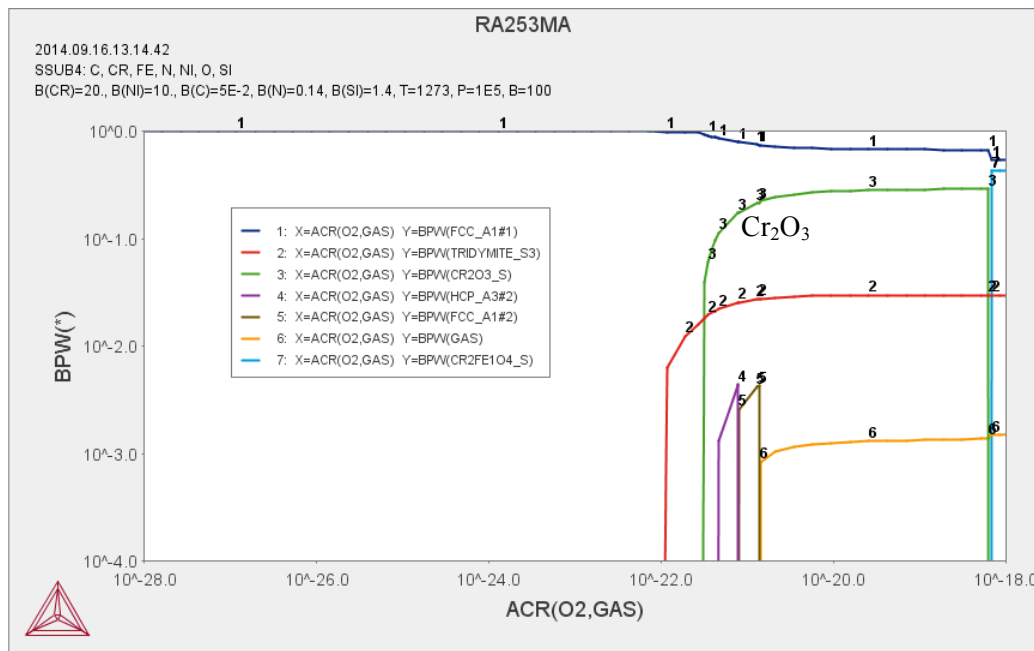


Figure 12. Formation of oxide layers on top of alloy RA253 MA at 1000°C. The thermodynamic activity of oxygen (fugacity) is plotted along the x-coordinate, while BPW(*) stands for the weight fraction of the different phases comprising a given steel, and oxides forming on the surface.

6. CONCLUSIONS AND PLANS FOR FUTURE RESEARCH

In this work, several lessons were learned related to functioning of real-life complex heterogeneous alloys in aggressive gaseous environments comprised of several gases:

- In order to select the “real-life” material for a particular application, all of the potential regimes in which it may function need to be studied quantitatively. This is required to avoid costly stoppages and potentially detrimental/catastrophic events during service;
- A typical guidance of the type “This material is suitable for high-temperature applications” is not sufficient as its applicability will also depend upon the environment(s) in which it may have to function;
- A simple thermodynamic approach was proposed in this paper that includes thermodynamic assessment of the possibility of different detrimental processes (e.g., oxidation, sulfidation, carburizing etc.);
- In the case of possibility of different oxide formation, the sequence in which said oxides will get deposited on the surface needs to be studied using the construction of oxide layers for different values of the oxygen thermodynamic activity; then a conclusion can be made about the possibility of the material passivation;
- Studying Ellingham-Richardson-Jeffes diagrams for individual elements in such oxidizing atmospheres as O_2 , a mixture of CO/CO_2 , or H_2/H_2O , is not sufficient for the proper material selection;
- Instead, generalized Ellingham diagram(s) need to be constructed for all potentially detrimental processes, e.g., oxidation, for every alloy component, in that particular gaseous atmosphere. This is how the research presented here will be continued.

Acknowledgments. The authors express their sincere gratitude to Drs. Ch. Jiang and P. Mason, of Thermo-Calc Software Inc. (McMurray, PA) for their assistance with conducting the calculations and expert advice.

7. REFERENCES

1. H.J.T. Ellingham, "Transactions and Communications", *J. Soc. Chem. Ind. (London)* vol. 63(5), p.125 (1944)
2. F.D. Richardson and J.H.E. Jeffes, "The Thermodynamics of Substances of Interest in Iron and Steel Making from 0°C to 2400°C: I - Oxides," *J. Iron and Steel Inst.*, vol.160 (1948) p.261
3. Peter Atkins, Julio de Paula, *Physical Chemistry: Thermodynamics and Kinetics*, 8th edition, W.H. Freeman, New York (2006)
4. E.T. Turkdogan, "Physical Chemistry of High Temperature Technology", Academic Press (1980)
5. A.S. Khanna, Introduction to High Temperature Oxidation and Corrosion, ASM International (2002)
6. M. Hillert, Phase Equilibria, Phase Diagrams, and Phase Transformations: Their Thermodynamic Basis, 2nd edition, Cambridge University Press, Cambridge (2008).
7. H.L. Lukas, S.G. Fries, and Bo Sundman, Computational Thermodynamics (The CALPHAD Method), Cambridge University Press, Cambridge (2007).
8. D.R. Gaskell, "Introduction to the Thermodynamics of Materials", Taylor and Francis (1995) 3rd edition; treatment of the Ellingham diagrams is described in pp.347-395)
9. A. Chirkin, Oxidation-induced phase transformations and lifetime limits of chromia-forming nickel-base alloy 625 [M.S. Thesis, RWTH, Aachen], December (2011).
10. M.V. Glazoff, S.N. Rashkeev, and J.S. Herring, Controlling chromium vaporization from interconnects with nickel coatings in solid oxide devices, *International Journal of Hydrogen Energy*, vol.39, pp.15031-15038 (2014)
11. Thermo-Calc Classic Version S User's Guide, P. Shi and B. Sundman, eds., Thermo-Calc Software AB, Stockholm, Sweden, 2010.
12. Superalloys for High-Temperature Applications – a Primer, ASM International, Metals Park, OH (2002)
13. M.V. Glazoff, A.Tokuhiro, S.N. Rashkeev, and P. Sabbharwall, Oxidation and Hydrogen Uptake in Zirconium, Zircaloy-2 and Zircaloy-4: Computational Thermodynamics and Ab Initio Calculations, *Journal of Nuclear Materials*, vol. 444, pp.65-75 (2014)
14. S. Lyon, Overview of Corrosion Engineering, Science, and Technology. In: Nuclear Corrosion Science and Engineering, ed. By D.Feron, Woodhead Publishing, Philadelphia (2012), p.20
15. Denny A. Jones, Principles and Prevention of Corrosion, New York (1992)
16. Gary S. Was, *Fundamentals of Radiation Materials Science*. Metals and Alloys, Springer, Berlin (2007)
17. K. Ishida and D.H. Lister, New model of cobalt activity accumulation on stainless steel piping surfaces under Boiling Water Reactor conditions, Proc. NPC 2010 Quebec City, Canada 3-7 October 2010
18. D.H. Lister, Understanding and mitigating corrosion in nuclear reactor systems. In: Nuclear Corrosion Science and Engineering, ed. By D.Feron, Woodhead Publishing, Philadelphia (2012), p.61

19. M.V. Glazoff, Thermodynamic Assessment of Hot Corrosion Mechanisms of Superalloys HastelloyTM N and Haynes 242 in Eutectic Mixture of Molten Salts KF and ZrF₄, INL External Report INL/EXT-12-24617, April 2012; rev.1 – September 2012
20. M.V. Glazoff, I. Charit, and P. Sabharwall, Computational Thermodynamic Modeling of Hot Corrosion of Alloys Haynes 242 and HastelloyTM N for KF-ZrF₄ Molten Salt Service in Advanced High Temperature Reactors, *Nuclear Energy Science and Power Generation Technology*, vol.3, issue 3, article 1000125, pp.1-11 (2014)

Appendix 1 Thermo-Calc Script for Calculating Chemical Potentials of Several Components in Alloy RA253 MA

```
go da
sw tcfe7
def-el fe cr ni si c n
get
go p-3

s-c p=1e5,n=1,t=1273
s-c w(cr)=0.20,w(ni)=0.10,w(si)=0.014,w(c)=0.0005,w(n)=0.0014
c-e
l-e
SCREEN
VWCS

set-ref-state fe fcc_a1 * 1E5
set-ref-state cr bcc_a2 * 1E5
set-ref-state ni fcc_a1 * 1E5
set-ref-state C graphite * 1E5
set-ref-state Si diamond * 1E5

show mur(fe)
show mur(cr)
show mur(ni)
show mur(si)
show mur(C)

set-inter
```

Appendix 2. Thermo-Calc Script for Calculating Chemical Potentials of Several Components in Gaseous Phase

```
go da
sw ssub5
d-sys N C O H S
get
go p-3
set-input-amount n(o2)=0.04 n(c1o2)=0.1 n(h2o1)=0.50
set-input-amount n(o2s1)=0.0001 n(n2)=0.3599
set-input-amount n(o3s1)=0.000002
s-c t=1273 p=1e5
c-e
l-e

set-ref-state C graphite * 1E5
set-ref-state O gas * 1E5
set-ref-state S gas * 1E5

show mur(C)
show mur(O)
show mur(S)

set-inter
```